Asian Journal of Current Research in Clinical Cancer
ISSN: 3062-4444
2025, Volume 5, Issue 2, Page No: 211-225

Available online at: www.galaxypub.co/page/journals

Galaxy Publication

Somatic Alterations in TP53 and KRAS and Their Functional Impact in Epithelial Ovarian Cancer

Lucas Meyer[1]*, Anna Schmid[2], Stefan Braun[1]

[1]Department of Oncology and Precision Cancer Medicine, Faculty of Medicine, ETH Zurich, Zurich, Switzerland.
[2]Department of Clinical Cancer Therapeutics, Faculty of Medicine, University of Bern, Bern, Switzerland.

***E-mail** ✉ lucas.meyer@gmail.com

Received: 07 August 2025; **Revised:** 25 October 2025; **Accepted:** 29 October 2025

ABSTRACT

In light of the bleak outlook for chemotherapy-resistant epithelial ovarian carcinoma (EOC) patients, we set out to corroborate the observations from an earlier whole-exome sequencing investigation by performing orthogonal Sanger sequencing on the identical patient cohort, along with an additional independent set of 127 EOC cases (n = 177, exclusively fresh frozen tumor specimens). Our emphasis was on TP53, a recurrently altered gene with implications for chemosensitivity, while KRAS was included as a supplementary therapeutic target; we further augmented the work with transcriptional expression data for both genes and assessed associations with clinical characteristics. Every TP53 and KRAS alteration uncovered by exome sequencing was verified. Individuals bearing KRAS mutations presented with a markedly higher prevalence of FIGO stages I or II (P = .002) and non-high-grade serous histological categories (nonHGSCs) (P < .001), which corresponded with diminished KRAS transcript abundance (P = .004). Those with non-HGSC classifications exhibited TP53 mutations less often (P = .002). Subjects carrying TP53 alterations that disturb the DNA binding loop experienced considerably prolonged platinum-free intervals relative to all other patients (P = .037). Tumor samples harboring nonsense, frameshift, or splice site TP53 alterations displayed markedly reduced TP53 transcript abundance, whereas samples with missense alterations showed significantly elevated levels in comparison to wild-type counterparts (P < .001). Normalized intratumoral transcript levels of TP53 and KRAS showed a correlation, and patients whose tumors harbored concurrent mutations in both genes had inferior overall survival compared with the remaining cohort (P = .015). Protein expression levels for both genes correlated meaningfully with their corresponding transcript measurements (P = .028 and P = .001, respectively). Our work designates KRAS as a candidate for forthcoming therapeutic strategies targeting non-HGSCs and highlights the prognostic relevance of TP53 alterations within the DNA-binding loop.

Keywords: Epithelial ovarian carcinoma, Platinum sensitivity, TP53, KRAS, Variant, Transcript expression

How to Cite This Article: Meyer L, Schmid A, Braun S. Somatic Alterations in TP53 and KRAS and Their Functional Impact in Epithelial Ovarian Cancer. Asian J Curr Res Clin Cancer. 2025;5(2):211-25. https://doi.org/10.51847/WMTWAtDFtw

Introduction

Epithelial ovarian cancer (EOC) ranks as the eighth most frequent contributor to cancer-associated mortality in women and represents among the deadliest gynecologic neoplasms [1]. Identifying EOC at an early stage is difficult, as the disease often remains symptom-free during its initial phases (stage I or II according to the International Federation of Gynecology and Obstetrics [FIGO] classification). Around 75% of EOC diagnoses occur at advanced stages (III or IV), at which point the 5-year survival estimate is roughly 20%–45%, compared with 40%–70% for stages I or II [2, 3]. The established therapeutic approach for advanced EOC has generally consisted of upfront cytoreductive surgery succeeded by platinum-based chemotherapy combined with paclitaxel

for the bulk of patients [4]. Nonetheless, the majority of individuals suffer recurrence within 5 years following initial diagnosis, and merely 20%–25% attain long-term remission [5].

Based on histomorphological features, EOCs are grouped into four principal subtypes: serous, endometrioid, clear cell, and mucinous [6]. An alternative classification separates them into two overarching categories: type I, which encompasses endometrioid, mucinous, clear cell, and low-grade serous ovarian carcinomas (LGSCs), and type II, which accounts for 70% of cases overall and includes high-grade serous ovarian carcinomas (HGSCs), carcinosarcomas, and undifferentiated carcinomas. These taxonomic frameworks are crucial for characterizing tumor aggressiveness and therapeutic responsiveness [3]. A predominant fraction, exceeding 80% of documented EOC instances, falls within the HGSC histological designation, distinguished by an aggressive biology tied to elevated death rates [7], a phenomenon ascribed not solely to detection at late stages but additionally to drug resistance, given that roughly half of advanced-stage cases recur within the initial 5-year window [3].

The emergence of Poly(ADP-ribose) polymerase (PARP) inhibitors, such as olaparib, and anti-angiogenic therapeutics, including bevacizumab and pazopanib, has brought significant prognostic advances for patients [8, 9]. PARP inhibitors (PARPis) are predominantly deployed as maintenance regimens for platinum-responsive advanced EOCs [10]. In addition, individuals with BRCA1/BRCA2 mutations exhibit greater sensitivity to PARPi agents [11].

Next-Generation Sequencing (NGS) enables cataloging of genetic diversity and its association with multidrug resistance. Genomic characterization has delineated two principal EOC varieties. Type I EOC features alterations concentrated in the MAPK signaling cascade (KRAS, BRAF, PTEN, and CTNNB1, among others), whereas type II is defined by mutations in TP53, BRCA1, BRCA2, KIT, and EGFR [12]. Furthermore, the DNA damage response machinery and associated defects in DNA repair pathways play a pivotal role in oncogenesis, including EOC. Germline alterations in DNA repair genes can signal heritable cancer syndromes, most notably BRCA1/2 mutations in breast and ovarian malignancies [13]. Pathogenic somatic mutations in genes within the homologous recombination DNA repair apparatus, including BRCA1/2, ATM, RAD51C, and RAD51D, have been linked to chemotherapy response and disease trajectory in EOC patients [14, 15]. HGSC characteristically exhibits an extraordinarily high rate of somatic TP53 mutations (approximately 90%) paired with extensive genomic variability [16].

Earlier whole-exome sequencing efforts [14] cemented TP53's standing as the most recurrently mutated gene across HGSC and EOC, while also implicating its role in chemosensitivity. Moreover, the subsequently assembled sample series, deliberately enriched with clear cell, mucinous, endometrioid, and low-grade serous carcinoma cases, demonstrated a strikingly elevated frequency of KRAS alterations (12% across all samples) [14], a finding suggestive of its relevance when formulating therapeutic strategies. The work presented here represents a follow-on validation study employing direct Sanger sequencing across both the initial and expanded sample cohorts, aimed at demonstrating the reliability of TP53 and KRAS mutation identification, providing confirmatory evidence for earlier results, and strengthening the case for their continued integration into everyday clinical decision-making. We further supplement somatic mutation profiling by measuring transcript levels for both genes in tumor-extracted RNA, alongside protein levels in a curated subset of specimens. These molecular readouts are then analyzed with respect to EOC treatment response and patient survival, thereby enabling assessment of the predictive and prognostic capacities of these biomarkers. Our investigation introduces an additional facet to previously published EOC research programs that drew upon exome or genome sequencing technologies [14, 17-19].

Materials and Methods

Patients

The tumor specimens underpinning this investigation were obtained at primary debulking surgery from 50 EOC cases with pre-existing whole-exome sequencing profiles (the confirmation set) [14] and a further 127 EOC cases for whom no exome data were available (the validation set). Recruitment was conducted prospectively across three hospitals in the Czech Republic—University Hospital Motol and University Hospital Královské Vinohrady, both situated in Prague, and University Hospital Pilsen—over an eleven-year window from 2009 to 2020. Freshly excised tumor tissue was immediately frozen and stored at −80°C until nucleic acid purification. A matched peripheral blood sample was collected from every participant, enabling paired tumor-germline comparisons.

Treating clinicians extracted from patient charts the following clinicopathological variables: age at diagnosis, FIGO stage (documented according to the pTNM classification system), histological subtype and tumor grade,

presence or absence of distant metastases and postoperative residual tumor, details of oncological treatment delivered, platinum sensitivity designation, and overall survival (OS). The categorization of platinum sensitivity was based on the platinum-free interval (PFI), defined as the time from cessation of platinum-based adjuvant chemotherapy to the earliest radiological or clinical evidence of relapse or progression [20]. Patients with a PFI of less than 6 months were classified as platinum-resistant; those with a PFI of 12 months or more were considered platinum-sensitive. Where PFI fell within the 7–12-month bracket, the designation partially platinum-sensitive was applied. For analytical purposes, these intermediate cases were initially assigned to the resistant stratum, and every statistical test of association was performed in duplicate, with and without their inclusion. Only findings that withstood both analytical approaches are presented below. OS was determined as the period separating the date of surgical resection from either death of any cause or the date at which the patient was last known to be alive. Exhaustive clinical characterization of the cohort is set out in **Table 1.**

The experimental framework of the study secured approval from the Institutional Review Boards of four bodies: the National Institute of Public Health in Prague (approval reference no. IGA NS9803–4, issued 2 February 2008), University Hospital Motol (approval reference no. EK-890/15, issued 24 June 2015), University Hospital Královské Vinohrady (approval reference no. EK-VP/40/0/2017, issued 28 June 2017), and University Hospital Pilsen (approval reference no. 16-29013A, issued 4 June 2015). Each individual whose data and biospecimens contributed to the study provided written informed consent by personally signing the Patient Informed Consent form after reviewing its contents.

Isolation of nucleic acids and cDNA synthesis

DNA extraction from peripheral blood lymphocytes was accomplished with the DNeasy Blood and Tissue Kit (Qiagen, Hilden, Germany). For solid tumor samples, frozen tissue was pulverized to a fine powder using a pre-cooled mortar and pestle under liquid nitrogen. The resultant powder was then processed through the AllPrep DNA/RNA/Protein Mini Kit (Qiagen) according to the supplier's instructions, permitting simultaneous recovery of total RNA and DNA from a single tissue aliquot. Quantitation of the isolated nucleic acids was performed fluorometrically on the Qubit 4 system (ThermoFisher Scientific, Waltham, MA, USA). The integrity of the RNA and DNA preparations was verified by measuring RIN and DIN, respectively, using the Agilent TapeStation 2200 platform (Thermo Fisher Scientific). Synthesis of first-strand cDNA from the RNA template was carried out with the RevertAid™ First Strand cDNA Synthesis kit (ThermoFisher Scientific) following the manufacturer's recommended workflow, and the resulting cDNA was quality-checked by a previously published protocol [21].

Gene expression analysis

Quantification of transcript abundance was performed by real-time quantitative PCR (qPCR) using predesigned TaqMan® Gene Expression Assays (Thermo Fisher) targeting TP53 (Hs01034249_m1) and KRAS (Hs00364284_g1). Normalization of expression values employed three stably expressed reference genes—PPIA (Hs99999904_m1), UBC (Hs00824723_m1), and YWHAZ (Hs03044281_g1)—which had been previously selected through systematic evaluation with the NormFinder and geNorm algorithms [22]. Each qPCR reaction totaled 5 µL and was composed of: 1 µL of 5× Hot FirePol Probe qPCR Mix Plus (ROX) (Solis BioDyne OÜ, Tartu, Estonia), 0.25 µL of the respective 20× TaqMan® Gene Expression Assay, 1.75 µL of nuclease-free water, and 2 µL of cDNA pre-diluted 8-fold. All reactions were arrayed in 384-well microplates and thermal cycling was executed on the ViiA7 Real-Time PCR System, with data captured and processed by the integrated ViiA7 System Software (Life Technologies, Carlsbad, CA, USA). The thermal profile began with a 2-minute hold at 50°C and a 10-minute initial denaturation at 95°C, followed by 45 amplification cycles, each consisting of a 15-second denaturation step at 95°C and a combined annealing/extension step at 60°C lasting 60 seconds. No-template control wells, in which the cDNA input was substituted with water, and negative reverse transcription controls (RNA subjected to the cDNA synthesis procedure without the inclusion of reverse transcriptase enzyme) were incorporated on every plate to rule out reagent contamination and genomic DNA carryover. All samples were assayed in duplicate; whenever the standard deviation between replicate Ct values exceeded 0.5 cycles, the sample was re-run. The entire qPCR workflow adhered strictly to the Minimum Information for Publication of Quantitative Real-Time PCR Experiments (MIQE) guidelines [23].

Between-sample and between-group expression differences were derived from raw Ct measurements by applying the comparative Ct framework [24]. The $2^{-\Delta Ct}$ method yielded relative gene expression values, while fold changes between groups defined by clinicopathological features, mutation carriage, or mutation classification were calculated using the $2^{-\Delta\Delta Ct}$ approach.

Direct sequencing

Sanger-based direct sequencing was performed for exons 2 and 3 of KRAS and exons 4-10 of TP53. In outline, target amplicons were first generated from genomic DNA by conventional PCR, each employing a primer pair tailored to the specific region (Online Resource 7). Successful amplification and appropriate product length were confirmed by agarose gel electrophoresis, after which amplicons were purified by ethanol precipitation. Each PCR was optimized beforehand to produce a clean, single-band amplification product. Purified PCR product (approximately 10 ng) was then combined with 2 pmol of the relevant sequencing primer in a final volume of 10 µL and subjected to cycle sequencing using the BigDye Terminator v3.1 Cycle Sequencing Kit (Invitrogen) in accordance with the manufacturer's instructions. Forward and reverse strands were sequenced independently (primer details in Online Resource 7). Post-reaction cleanup was performed using ExoSAP-IT™ PCR Product Cleanup Reagent (Applied Biosystems, Foster City, CA). Capillary electrophoresis and base calling were performed on a commercial basis by SEQme, s.r.o. (Dobris, Czech Republic). Raw electropherograms were examined and curated using the BioEdit 7.2.5 software package in conjunction with Sequencing Analysis Software v5.2 (Applied Biosystems). All oligonucleotide primers deployed for amplification and sequencing (Online Resource 7) were designed with the Primer3 program [25].

Immunoblotting

For protein-level analyses, 52 tumor specimens were deliberately selected to span the extremes of transcript expression—capturing both the most abundant and least abundant signals—while simultaneously covering a diverse array of KRAS and TP53 mutation types. Total protein was recovered from patient material using the AllPrep DNA/RNA/Protein Mini Kit (Qiagen), and protein concentrations were determined in all lysates using the Pierce™ BCA Protein Assay Kit (Thermo Fisher Scientific). To enable signal normalization between individual blots, a lysate prepared from the Panc-1 pancreatic cancer cell line—previously established to express both KRAS and p53 at appreciable levels—was included as a standardizing reference on each of the four membranes. Per lane, 20 µg of total protein was fractionated by electrophoresis through a 12% (w/v) polyacrylamide gel under denaturing conditions (SDS-PAGE), then wet-transferred to a nitrocellulose membrane. After completing the transfer step, each membrane was physically divided into two segments. The upper segment was blocked for 1 hour in Blocker™ BLOTTO formulated in TBS buffer (Thermo Fisher Scientific). It was then submerged overnight at 4°C in a solution containing two primary antibodies combined: one targeting p53 (mouse monoclonal, A10610, Abclonal Science, Düsseldorf, Germany) and another recognizing the housekeeping protein GAPDH, which functioned as the internal loading reference (rabbit monoclonal, 14C10, #2118, Cell Signaling Technology, MA, USA). Both antibodies were diluted in Blocker™ BLOTTO in TBS containing 0.2% (v/v) Tween®20. The lower membrane segment was handled identically, except that the primary antibody solution contained only the anti-KRAS reagent (rabbit polyclonal, GTX100636, GeneTex, CA, USA). After thorough rinsing with TBS supplemented with 0.1% (v/v) Tween®20, each segment was incubated with fluorophore-conjugated secondary antibodies for 1 hour at room temperature. The upper segment received a dual-color detection mix consisting of IRDye® 800CW Goat anti-Mouse IgG plus IRDye® 680RD Goat anti-Rabbit IgG (Li-Cor, Lincoln, NE, USA).

In contrast, the lower segment was treated with IRDye® 800CW Goat anti-Rabbit IgG alone. Immunoreactive bands were visualized by infrared fluorescence scanning on the Odyssey® Fc Imaging System (Li-Cor), and band intensities were digitized and quantified using Image Studio software, version 4.0.21 (Li-Cor). Uncropped scans of the membranes, with the areas excerpted for **Figure 1d** clearly demarcated, are supplied in Online Resource 8.

External datasets

To seek independent confirmation of the somatic variants detected in TP53 and KRAS, we drew upon the American Association for Cancer Research (AACR) Genomics Evidence Neoplasia Information Exchange (GENIE) version 15.0-public, which became available on 1 February 2024 and compiles targeted panel sequencing results contributed by numerous prominent oncology centers [26]. From this repository, only entries meeting each of the following criteria were retained: histology consistent with EOC, specimen type listed as primary tumor, at least one somatic mutation call retrievable upon sample ID-based matching, and the specific gene(s) under investigation (TP53 and/or KRAS) represented on the gene panel used for that particular sample. The final filtered GENIE set numbered 2210 samples. For the separate task of validating transcriptional and mutational findings with orthogonal data, we downloaded the GDC TCGA-OV cohort from the University of

California, Santa Cruz Xenabrowser portal (https://xenabrowser.net). RNAseq-based gene expression values (normalized to FPKM-UQ) and DNAseq somatic mutation annotations (generated with the Mutect2 pipeline) were extracted and restricted to specimens designated as primary ovarian tumors, yielding a total of 374 samples. It should be noted that this dataset lacks representation of rarer histological subtypes and provides no refined histopathological subclassification beyond a uniform assignment to the serous category; accordingly, subtype-stratified analyses were not possible with this resource.

Statistical analysis

Potential links between categorical clinical descriptors (FIGO stage, tumor grade, extent of residual disease after surgery, chemosensitivity assignment) and the functional categorization of mutations were explored using either the Pearson chi-square statistic or, in instances where expected cell frequencies were low, Fisher's exact test. Continuous variables—such as age at diagnosis or normalized transcript levels—were compared across categorical groupings using the Kruskal–Wallis nonparametric test. The strength and direction of associations between pairs of continuous measures were evaluated using Spearman's rank correlation coefficient (rho). All statistical tests were two-sided, and the threshold for significance was set at $P < 0.05$. Graphical depiction of survival experience by group relied on the Kaplan–Meier product-limit estimator. Expression data were partitioned into quartile-based strata, and the cut-point delivering the most pronounced separation between survival curves, as gauged by the log-rank statistic, was designated the optimal cut-off. The entire statistical analysis was conducted in SPSS v16 (SPSS, Chicago, IL, USA). A preceding draft of this manuscript was made publicly accessible through the ResearchSquare preprint platform [27]. The present article represents a considerably reworked and updated version of that earlier communication.

Results and Discussion

Patients' characteristics

The defining clinical and demographic features of the entire study population (N = 177) are presented in **Table 1.** At the time of diagnosis, the median age was 62 years (range 24-89). The great majority of individuals fell into the categories of FIGO stage III (82%), histological grade G3 (85%), and the HGSC subtype (84%). Approximately one patient in three (32%) had been treated with chemotherapy before surgical intervention, while one in two (50%) were documented as having tumor residuum persisting after cytoreductive surgery. Platinum-containing combination chemotherapy was administered in the adjuvant setting to nearly the entire cohort (96%); two individuals received taxane monotherapy, four received no adjuvant systemic treatment due to poor performance status, and therapeutic information could not be retrieved for six individuals. The median PFI and OS were recorded at 25 and 48 months, respectively. Those presenting with FIGO stage III or IV, postsurgical residual tumor (R1 or R2), or a PFI of less than 12 months experienced a significantly shorter OS than the remainder of the cohort ($P < .001$ for each comparison) (Online Resource 1A-C).

Table 1. Clinical characteristics of EOC patients.

Parameters	Percentage	Number of patients
Age at diagnosis	100	177
Median ± SD (years)	62.0 ± 11.5	
FIGO stage		
I	7	12
II	6	10
III	82	139
IV	5	8
Data not available	–	8
Histologic grade (G)		
G1	6	11
G2	9	15
G3	85	146
Gx	–	5
Tumor subtype		
HGSC	84	143
Other*	16	28

Data not available	–	6
Distant metastasis		
Absent	95	161
Present	5	8
Data not available	–	8
Neoadjuvant chemotherapy		
Administered	32	57
Not administered	68	120
Residuum after surgery		
Present**	50	85
Absent (R0)	50	85
Data not available	–	7
Adjuvant chemotherapy		
Platinum-based#	96	165
Taxane monotherapy	1	2
Not administered	3	4
Data not available	–	6
Chemosensitivity status		
Resistant (PFI ≤ 6 months)	23	38
Intermediate (PFI 7–11 months)	15	24
Sensitive (PFI ≥ 12 months)	62	101
Data not available	–	14
Platinum-free interval	95	168
Median ± 95% confidence interval (months)	17.9–32.1	25
Overall survival	95	168
Median ± 95% confidence interval (months)	37.7–58.3	48

Other subtypes include the following carcinomas: mucinous (n = 9), clear cell (n = 10), low-grade serous (n = 5), endometrioid (n = 2), and borderline (n = 2).

Includes all ratings above R0 (R1, R2, unspecified).

#Platinum-based chemotherapy regimens include n = 147 taxane (paclitaxel/docetaxel) with platinum (carboplatin/cisplatin), n = 9 platinum monotherapy, other (n = 1 FOLFOX, n = 1 platinum with anthracycline, n = 1 platinum with paclitaxel and anthracycline, and n = 6 platinum with paclitaxel and cyclophosphamide). FOLFOX = 5-fluorouracil, leucovorin, and oxaliplatin.

Somatic genetic variability

The full set of six KRAS alterations previously identified via exome sequencing (n = 50) was likewise successfully identified by Sanger sequencing in the confirmatory subset (n = 50). Across the larger validation subset (n = 125, noting that two specimens could not be processed owing to inadequate DNA), alterations were uncovered in a further nine tumor specimens **(Table 2).** Each alteration constituted a missense single-nucleotide substitution, mapping to either exon 2 (n = 12) or exon 3 (n = 3). Characteristic chromatogram traces are supplied in Online Resource 2A, B.

Table 2. Molecular characteristics of EOC patients.

Gene	Percentage	Number of patients
KRAS mutation status*		
KRAS wild-type	93	161
KRAS mutated	8	15
KRAS mutation spectrum		
p.Gly12Asp	33	5
p.Gly12Val	33	5
p.Gln61His	13	2
p.Gly12Cys	7	1
p.Gly12Ala	7	1
p.Gln61Arg	7	1
TP53 mutation status		
TP53 wild-type	41	72
TP53 mutated	59	105
TP53 mutation spectrum		

Hotspots		
p.Arg175His		8
p.Tyr220Cys		7
p.Arg273His		6
p.Arg248Gln		5
p.Arg248Trp		4
p.Arg282Trp		4
p.His214Arg		3
p.His179Gln		2
p.Arg249Trp		2
p.Cys275Phe		2
p.Gly279Glu		2
p.Glu198Ter		3
p.Arg213Ter		3
Private missense mutations		32
Private frameshift or nonsense mutations		17
Private splice site mutations with pathogenic features		5
***TP53* mutation functional consequences#**		
Loss-of-function	92	87
Gain-of-function	8	8
Not classified	–	10
Dominant-negative effect (DNE) & loss-of-function (LOF) properties#		
DNE_LOF	86	66
notDNE_notLOF	7	5
notDNE_LOF	7	5
Not classified	–	29
Transactivation function#		
Non-functional	90	64
Functional or partially functional	10	7
Not classified	–	34
DNA binding loop affected#		
Yes	94	94
No	6	6
Not applicable	–	5

Result for two samples not available due to DNA of low quality/quantity.
#Evaluated using The TP53 database of NCI (https://tp53.isb-cgc.org/.) and The Clinical Knowledgebase (https://ckb-core.genomenon.com/) and literature cited therein.

Shifting focus to TP53, the confirmatory subset yielded an exact mirror of the exome sequencing output, with 39 mutant and 10 wild-type cases identified. In the validation subset (n = 127), an additional 66 mutant samples were brought to light **(Table 2).** Archetypal chromatogram traces appear in Online Resource 3A-K.

Functional annotation allowed the grouping of TP53 alterations into several discrete classes: i/missense substitutions (n = 77), of which 32 represented isolated private mutations and the remainder constituted mutational hotspots detected across two or more individuals, ii/two hotspot nonsense substitutions each encountered in three individuals, and iii/private frameshift or nonsense substitutions (n = 17). A concluding class encompassed splice-site substitutions with predicted pathogenic consequences, each of which was found to be private (n = 5). Employing the TP53 database from NCI, together with the Clinical Knowledgebase (CKB), enabled a more granular separation into loss-of-function (n = 87) versus gain-of-function (n = 8) variants. When cross-referenced against these curated resources, most somatic variants received the following property assignments: dominant-negative effect or loss-of-function (n = 66), transcriptionally inactive (n = 64), and disruptive to the DNA binding loop (n = 94) **(Table 2)** (Online Resource 4).

Four individuals were found to have simultaneous TP53 and KRAS mutations (co-mutations). One, whose tumor was subtyped as HGSC, harbored the TP53-Arg282Trp plus KRAS-Gln61His pairing, was deemed chemoresistant, and survived 16 months overall. A second, bearing clear cell histology, showed the TP53-Arg248Gln plus KRAS-Gln61Arg combination, likewise chemoresistant, with an overall survival of only 7 months. A third of the mucinous subtype, which carried TP53-Arg213Ter paired with KRAS-Gly12Asp, exhibited

chemoresistance and had an OS of 19 months. The fourth and final co-mutated case showcased TP53-Cys135Trp alongside KRAS-Gly12Val, HGSC histology, a chemosensitive classification, and an OS reaching 43 months. These observations raise the possibility that joint carriage of TP53-KRAS alterations may correlate with treatment resistance and an unfavorable disease trajectory in the majority of cases.

All clinical genomic analyses conducted from this point onward drew upon the unified confirmation and validation cohorts (n = 177).

Intratumoral KRAS and TP53 transcript and protein levels

To obtain complementary functional data, we employed qPCR to quantify TP53 and KRAS transcript levels in each tumor specimen for which both genetic data and suitable material were available. Five specimens could not be quantified due to insufficient RNA quantity or purity, combined with depleted tissue stocks. No values fell into the extreme outlier range.

Neither the existence nor the specific class of KRAS alteration bore any statistically significant relationship to the transcript quantities measured for either KRAS or TP53 ($P > .05$). A markedly different picture emerged for TP53: tumors with nonsense, frameshift, or splice site alteration classes demonstrated transcript quantities that fell substantially below those seen in TP53 wild-type tumors ($P < .001$) **(Figure 1a).** In stark contrast, specimens harboring missense TP53 alterations showed transcript levels that were well above wild-type levels ($P < .001$) **(Figure 1a).** Additionally, transcript abundance was more pronounced in tumors whose TP53 alterations had been categorized as gain-of-function relative to those deemed loss-of-function ($P = .027$) **(Figure 1b).**

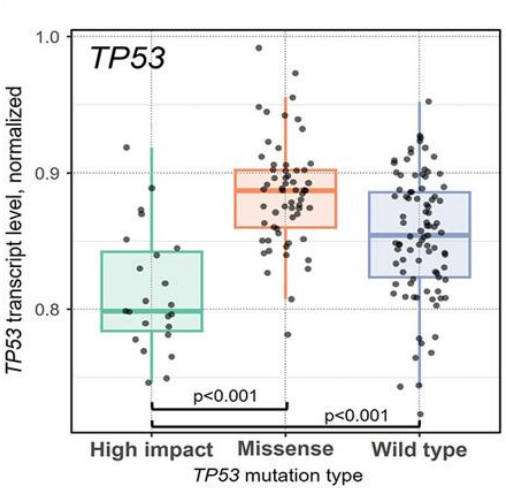

a)

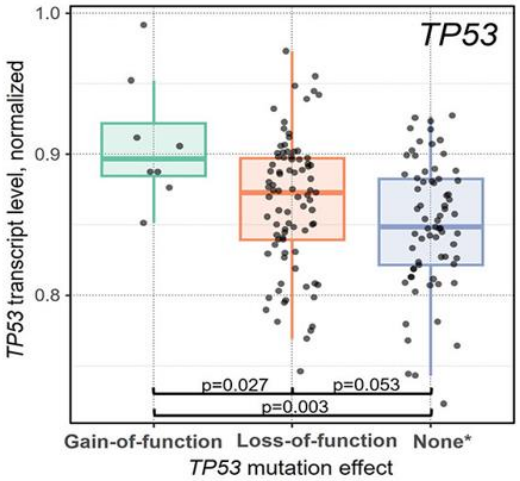

b)

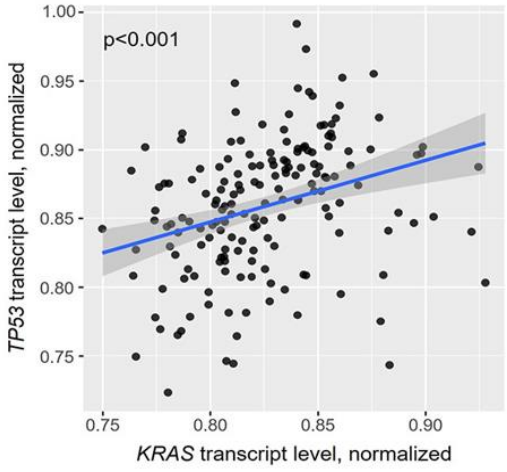

c)

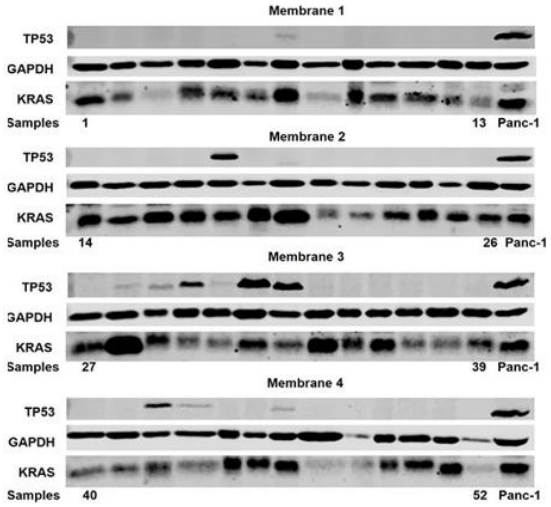

d)

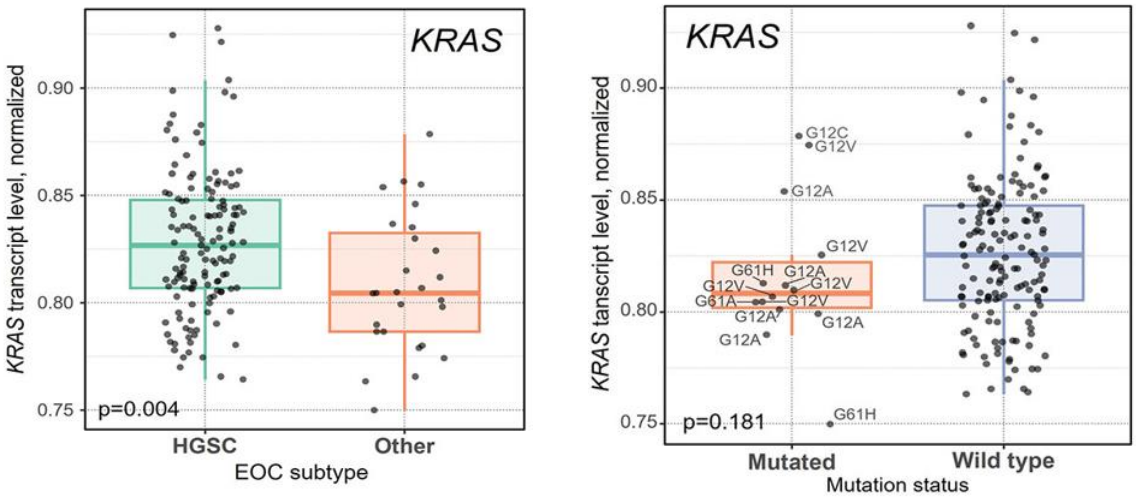

e) f)

Figure 1. Associations of TP53 and KRAS normalized transcript levels in tumors with characteristics of EOC patients: (a) TP53 normalized transcript level with TP53 mutation type, (b) effect (gain-of-function vs. loss-of-function), (c) Mutual correlation between KRAS and TP53 transcript levels, (d) Four membranes representing KRAS and p53 protein levels with GAPDH loading control and Panc-1 cell line for inter-membrane normalization, (e) KRAS normalized transcript level with EOC subtype, and (f) mutation status. High-impact means nonsense, frameshift, or splice-site functional variant classification. Footnote: 5 high-impact and 4 missense variants could not be classified and are excluded from the plot. Harboring co-mutated TP53-KRAS exerted no detectable influence upon transcript expression (p = .096 for TP53 and p = .306 for KRAS).

A particularly intriguing result emerged from the observation that normalized intratumoral TP53 and KRAS transcript quantities exhibited a robust reciprocal correlation ($\rho = 0.384$, $P < .001$) **(Figure 1c).** In line with this, KRAS protein abundance **(Figure 1d),** as measured through immunoblotting, corresponded meaningfully with its cognate transcript abundance ($n = 52$, $\rho = 0.305$ and $P = .028$). For p53 protein **(Figure 1d)** relative to its transcript, this correspondence attained an even greater degree of strength ($n = 52$, $\rho = 0.431$ and $P = .001$). KRAS and p53 protein abundances, however, showed a complete absence of correlation with one another ($P = .804$).

Correlating somatic mutation profiles and transcript abundance with patient clinical parameters

The next phase of our analytical pipeline involved statistical interrogation of how transcript quantities, mutation presence and type, and functional annotation of both genes related to the clinical characteristics documented across the cohort.

A significantly greater proportion of patients diagnosed at FIGO stage I or II carried KRAS mutations than those with stage III or IV disease ($P = .002$) **(Table 3).** Looking at the matter from the opposite angle, individuals whose tumors fell under the HGSC classification had a significantly diminished likelihood of bearing either KRAS or TP53 mutations ($P < .001$ and $p = .002$, respectively) **(Table 3),** yet their tumors yielded significantly richer KRAS transcript signals ($P = .004$) **(Figure 1e)** relative to the other histological subtypes. It should be noted, however, that KRAS transcript quantity was entirely independent of whether the gene was mutated or not ($P = .181$) **(Figure 1f)**. Across the board, neither the mutational status, spectrum, nor transcript quantity of KRAS demonstrated any meaningful link with the additional clinical covariates examined (age, tumor grade, extent of surgical cytoreduction, chemosensitivity, PFI, or OS; all $P > .05$), a statement that applied equally to the relationship between transcript quantity and FIGO stage.

Table 3. Associations between KRAS mutational status and stage or tumor subtype of EOC patients.

Characteristics	P-value	KRAS mutated*	KRAS wild-type*
Stage I/II	.002	6	16
Stage III/IV		7	139
HGSC	< .001	4	139
other subtypes		10	18

	P-value	TP53 mutated*	TP53 wild-type*
HGSC	.002	93	50
other subtypes		9	19

Number of patients: for some patients, clinical data or KRAS mutation status were unavailable.

Shifting attention to TP53, neither its transcript quantity, the mere presence of a mutation, the mutational spectrum, nor the assigned functional category bore any significant relationship to the clinical covariates under study (age, stage, tumor grade, subtype, surgical radicality, chemosensitivity status, or OS; all P > .05). One noteworthy exception did surface: patients whose TP53 alterations fell outside the DNA binding loop domain (n = 6) experienced a significantly briefer PFI than those whose mutations localized within this structural element (P = .037) **(Figure 2a).** Patients with TP53 and KRAS mutations had a significantly shorter OS than wild-type individuals or those with mutations in only one of the two genes (P = .015) **(Figure 2b).** However, the difference in PFI fell just shy of the conventional threshold for statistical significance (P = .065) **(Figure 2c).**

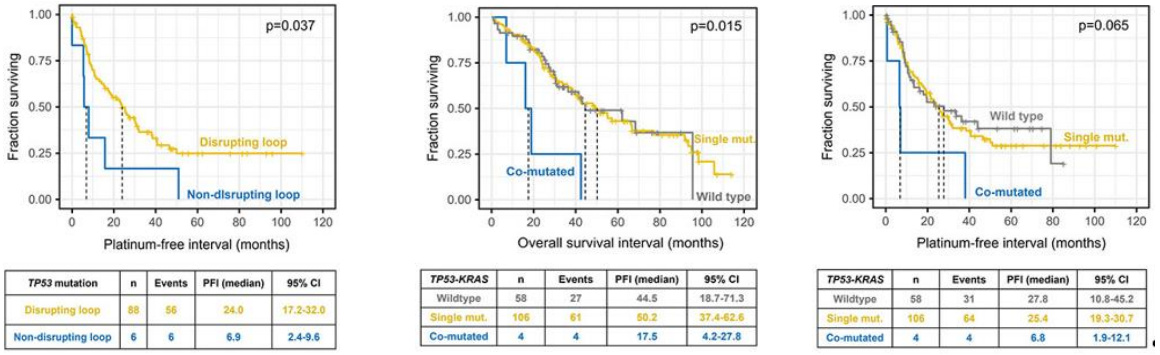

TP53 mutation	n	Events	PFI (median)	95% CI
Disrupting loop	88	56	24.0	17.2-32.0
Non-disrupting loop	6	6	6.9	2.4-9.6

TP53-KRAS	n	Events	PFI (median)	95% CI
Wildtype	58	27	44.5	18.7-71.3
Single mut.	106	61	50.2	37.4-62.6
Co-mutated	4	4	17.5	4.2-27.8

TP53-KRAS	n	Events	PFI (median)	95% CI
Wildtype	58	31	27.8	10.8-45.2
Single mut.	106	64	25.4	19.3-30.7
Co-mutated	4	4	6.8	1.9-12.1

a) b) c)

Figure 2. Associations between patient survival and carriage of TP53 or KRAS mutations: (a) Platinum-free interval stratified by carriage of TP53 DNA binding loop mutations in EOC patients, (b) overall survival and platinum-free interval, and (c) in TP53-KRAS co-mutated patients compared to wild-type or single gene mutated EOC patients.

Given the weight that EOC subtype carried in our earlier analyses, we divided the cohort into HGSC and non-HGSC strata. Members of the nonHGSC category were significantly more likely to harbor earlier-stage (I/II) disease than the HGSC group (P < .001, Online Resource 5), consistent with a less aggressive clinical picture. That said, when it came to PFI, only the clear cell subset (n = 10) fared discernibly better than the HGSC benchmark (n = 134), whereas mucinous (n = 9) and LGSC (n = 5) cases did not, and endometrioid cases (n = 2) actually registered the least favorable PFI figures (Online Resource 6A). These subtype-driven variations, however, did not yield meaningful differences in survival outcomes (Online Resource 6B).

Within the HGSC-restricted stratum (n = 143), no significant associations emerged between any clinical endpoint and KRAS or TP53 transcript quantities, mutation status, or functional designations. In the nonHGSC stratum (n = 28), by contrast, a non-significant tendency toward abbreviated PFI was observed among patients positive for any TP53 alteration relative to those with wild-type TP53 (P = .062). No relationship was detected for OS or any other clinical parameter, including chemosensitivity status.

Confirmatory analyses drawing on publicly available external cohorts

To round out our investigation, we endeavored to reinforce our principal observations by interrogating the most expansive and contemporaneous publicly accessible EOC collection, namely the GENIE project dataset (n = 2210).

Scrutiny of TP53 and KRAS alterations within this external resource confirmed the disproportionate enrichment of KRAS mutations among non-HGSC relative to HGSC specimens. Within our series, KRAS mutations were present in 32% of non-HGSC tumors, compared with only 1.4% in HGSC tumors. The sheer magnitude of the GENIE compilation enabled a breakdown of KRAS mutation prevalence across the principal non-HGSC entities. KRAS mutation frequency rose along a gradient as follows: HGSC (1.2%) << clear cell (13%) < endometrioid (27%) = LGSC (28%) < mucinous (67%). A parallel finding of equal or greater interest was the gradation in the

ratio of TP53 to KRAS mutability across subtypes: mucinous and clear cell tumors each exhibited a ratio approximating 1/1, whereas endometrioid and LGSC tumors harbored a greater absolute number of KRAS than TP53 mutations. Among HGSC tumors, the ratio stood at almost 100/1 in TP53's favor. Perhaps the single most thought-provoking result from the GENIE exploration was the discovery that a substantial subset of patients harbored simultaneous TP53 and KRAS alterations, with marked disparities across subtypes. Nearly half (46%) of all mucinous subtype patients carried mutations in both genes concurrently. The remaining subtypes showed substantially lower co-mutation rates: 4% among endometrioid cases and 1.5% among clear cell cases. Within LGSC and HGSC, the phenomenon occurred at comparable, negligible rates, each less than 1% **(Figure 3a).**

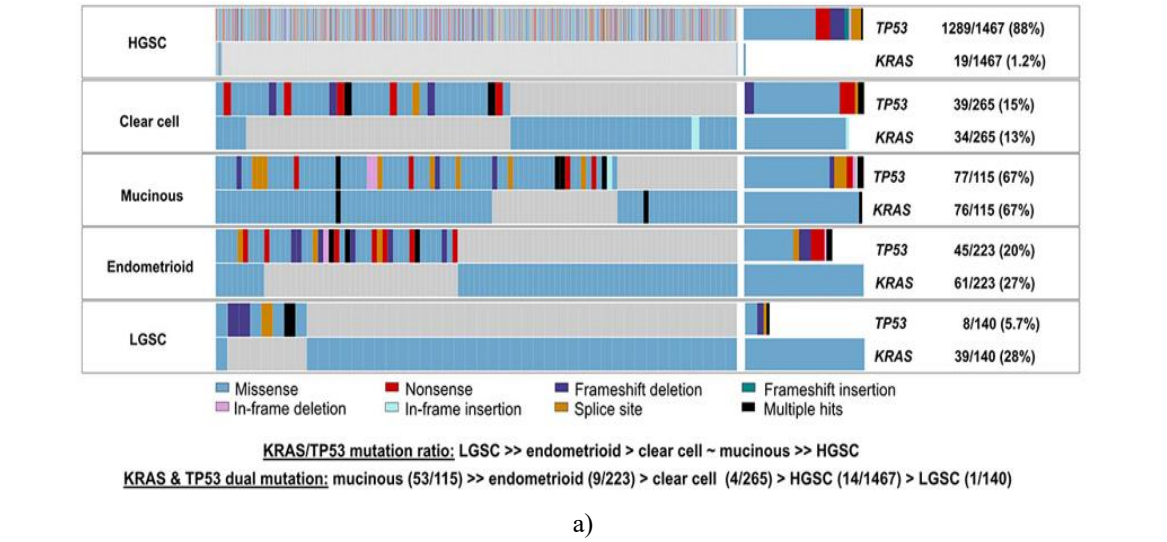

a)

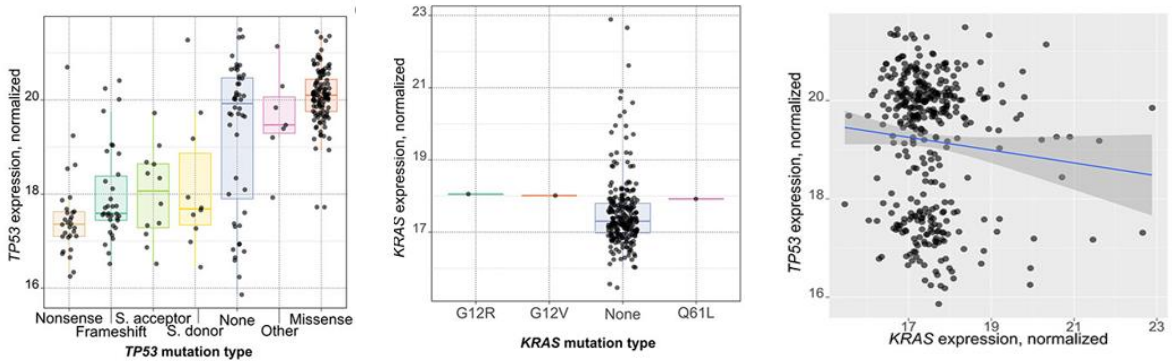

b) c) d)

Figure 3. Validation of TP53 and KRAS mutational spectra and intratumoral transcript levels in EOC subtypes using external datasets: (a) TP53 and KRAS mutational spectra in EOC subtypes, (b) TP53, (c) KRAS intratumoral transcript levels were stratified by their mutation type or classification, and (d) Correlation between TP53 and KRAS intratumoral transcript levels (lack of mutual correlation).

Because transcriptional information is not captured in GENIE, we used the TCGA-OV collection (n = 374) to assess transcript levels. Putting TP53 transcript abundance side by side with the core mutation classification groupings lent further support to the pattern we had earlier identified: transcript abundance was significantly elevated in specimens harboring missense mutations (P = .002) and significantly depressed in those with nonsense, frameshift, or splice-altering mutations (P = .009), using wild-type levels as the reference **(Figure 3b).** For KRAS, no meaningful association between transcript expression and the mutational spectrum emerged (P > .05) **(Figure 3c)**, a null result that could plausibly be attributed to the very sparse representation of mutated samples (n = 3). A modest correlation, failing to reach statistical significance (P = .052), was observed between TP53 and KRAS transcript levels **(Figure 3d).** Turning to the clinical annotations at hand, neither histological grade (G1/G2 pooled vs. G3/G4) nor stage (I/II vs. III/IV) exhibited a significant relationship with either KRAS or TP53 transcript abundance (P > .05, data not shown).

A search of the TCGA repository yielded only 2 instances of simultaneous KRAS-TP53 mutation. The first such case (TCGA-29–1696-01A) involved a KRAS Gly12Arg alteration partnered with a frameshift TP53 mutation;

this patient presented with stage IIIC, G2 disease and died at 34 months from the time of diagnosis. The second case (TCGA-61–2009-01A) featured a KRAS Glu61Leu alteration accompanied by a missense TP53 mutation; this individual had stage IIIC, G3 disease and was alive at the 40-month mark following diagnosis. Taken together, the external evidence does not appear to strengthen our single-institution observation that the three EOC patients carrying analogous co-mutations faced a considerably bleaker prognosis.

Given that the publicly accessible version of GENIE omits survival endpoints and that the TCGA dataset lacks histopathologically resolved subtype annotations (though every tumor in it is designated as serous), we were unable to replicate the prognostic associations identified in our study.

By deploying a benchmark direct sequencing technique, the investigation at hand verifies that mutations in TP53 and KRAS—two EOC driver genes with direct therapeutic relevance—are indeed present, as previously flagged by whole-exome sequencing of an initial 50-patient set. Expanding the inquiry, we sequenced both genes in an additional 127 EOC cases and layered somatic genotype data with transcriptomic profiling, aiming to extract richer functional insights.

A consistent thread running through the findings is that what a mutation does functionally and in which histological context it occurs eclipses the mere fact of its presence. Unpicking these dimensions thoroughly is a prerequisite to any sound clinical application. To illustrate with a concrete distinction, HGSC is characterized by TP53 alterations, whereas KRAS alterations are far more consequential in non-HGSC disease. This dichotomy aligns with widely held views [28] and may influence patient care [29]. The enrichment of KRAS mutations we observed in stage I/II presentations aligns with the observation that certain non-HGSC forms tend to be diagnosed at earlier stages than HGSC [30]. Yet this stage shift manifested as a non-significant PFI advantage exclusively within the clear cell group and only weakly modulated overall prognosis, as measured by OS. One must, however, factor in that clear cell carcinoma is generally considered less susceptible to platinum-based chemotherapy than other EOC subtypes [31], which suggests that our observation may be a function of the modest sample size ($n = 10$). The widespread prevalence of KRAS mutations across non-HGSC subtypes makes a strong case for enrolling these patients in forthcoming trials of emerging KRAS inhibitors. Preclinical and early clinical efforts with KRAS-G12D (MRTX1133) [32] and pan-KRAS [33] inhibitors are generating encouraging data, and agents targeting KRAS-G12C have already crossed the threshold into approved personalized therapy. Sotorasib is now sanctioned for targeted treatment of non-small cell lung cancer (NSCLC) [34], and adagrasib holds approval for both NSCLC and colorectal carcinoma [35].

The bearing of so-called loss-of-function and gain-of-function TP53 variant classifications [36] on disease course and on potential therapeutic exploitation has attracted prior debate [37]. Drawing on the TP53 database and the Clinical Knowledgebase, we therefore stratified subjects into subsets based on variants grouped by predicted functional consequence **(Table 2),** apart from variants that compromise the DNA-binding loop—which proved informative for a prolonged PFI—no other stratification scheme translated into discernible clinical differences.

What may constitute the most salient takeaway for current discussions around targeted and immunotherapeutic strategies emerged from the scrutiny of tumors jointly mutated in KRAS and TP53. Earlier reports in NSCLC [38, 39] and pancreatic carcinoma [40] have painted an inconsistent picture. While both sets of investigators documented the grim outlook tied to dual-mutant status, NSCLC has been portrayed as immunologically “hot,” in contradistinction to pancreatic carcinoma, which is regarded as “cold”—a divergence that carries implications for how these tumor types might respond to immune checkpoint blockade. Our data suggest that EOC could be a meaningful addition to this line of inquiry, as the co-mutated patients in our series ($n = 4$) experienced a significantly shorter OS, aligning EOC more closely with pancreatic cancer on this point.

Probing intratumoral transcript abundance for TP53 and KRAS revealed multiple meaningful patterns. Firstly, the two transcript measurements were significantly correlated. Secondly, TP53 transcript abundance faithfully mirrored the gene’s mutational architecture: tumors of missense variant carriers yielded higher levels, whereas those with other variant types—categorized as exerting high predicted functional impact—registered levels below the wild-type comparator ($P < .001$). In keeping with this, loss-of-function variants were associated with lower transcript levels than gain-of-function variants. Thirdly, and of no small consequence, non-HGSC tumors showed significantly lower KRAS transcript levels than HGSC tumors. Yet, within this subgroup, no coupling between mutation status and transcript level was detected, suggesting more layered regulatory inputs, possibly of an epigenetic nature. Both KRAS and p53 protein levels corresponded with their respective transcript levels, lending additional credence to the functional significance of measuring the transcriptome.

Drawing on the GENIE dataset ($n = 2210$) [26] for external corroboration enabled us to substantiate the observed interplay between TP53 mutation class and transcript output. More critically, it afforded a higher-resolution view

of how TP53 and KRAS mutation status varies across the histological spectrum of EOC. This dissection exposed a progressive shift in the TP53-to-KRAS mutability ratio, running as follows: HGSC >> clear cell ≈ mucinous > endometrioid >> LGSC. An even sharper gradient emerged when examining the frequency with which TP53 and KRAS are co-mutated: mucinous (53/115) >> endometrioid (9/223) > clear cell (4/265) > HGSC (14/1467) > LGSC (1/140). Although the high incidence of dual mutations in the mucinous subtype has been noted before [41], both trends highlight the extraordinary heterogeneity among EOC subtypes. This heterogeneity begs to be harnessed to support individualized treatment strategies.

Several limitations attached to this work warrant explicit mention. To begin with, the modest cohort size impedes a statistically robust exploration of non-HGSC subtypes, each of which constitutes a small fraction of EOC cases (under 10% apiece). Unfortunately, severe deficits in clinical data availability—GENIE omits survival information [26] and TCGA lacks EOC subtype annotation—prevented us from pursuing external replication of results that may have clinical relevance. Further studies in this space are therefore essential, and our contribution may feed into future meta-analytical syntheses. A second consideration is that the patients whose samples underpin this study received no PARPi or other targeted agents. Platinum-based chemotherapy remains the backbone of EOC treatment [42], and chemosensitivity to platinum and to PARPi shows considerable overlap [43, 44]. Viewed through this lens, our sample collection remains pertinent. A third point concerns the imperfect correlation between transcript levels and immunohistochemically assessed protein levels. It bears noting, however, that while immunohistochemistry is firmly embedded in routine clinical TP53 assessment, the same cannot be said for KRAS, where therapeutic decisions around EGFR blockade rest entirely on mutation status, and functional validation—especially for infrequently encountered variants—remains absent. Our work indicates this gap deserves greater attention. On the positive side, the present study draws strength from an ethnically homogeneous population, a standardized treatment protocol, and exhaustive longitudinal clinical follow-up.

Conclusion

In summation, our study reinforces earlier evidence positioning KRAS as a legitimate and, with any luck, imminently druggable vulnerability in non-HGSC EOCs, while simultaneously highlighting the prognostic significance of TP53 mutations in the DNA-binding loop for a defined subset of patients. Beyond that, we highlight a striking concentration of TP53-KRAS co-mutations in the mucinous form of EOC, a finding derived from interrogation of an external repository of 2210 samples. Our results collectively expand the aperture of precision oncology in EOC and lay down markers for where subsequent functional and preclinical investigations should head.

Acknowledgments: The authors would like to thank all participating patients for their kind consent to the study and the clinical personnel for their outstanding support.

Conceptualization – R.V. & P.S. Methodology – M.A., E.A., I.K., V.H., A.S., & F.A. Formal Analysis – P.H., R.V., & P.S. Investigation – M.A., E.A., V.H., A.S., & I.K. Resources – L.R., M.H., M.M., K.K., A.B., & J.B. Writing – Original Draft – M.A., R.V., & P.S. Writing – Review & Editing – M.A., E.A., I.K., P.H., V.H., F.A., L.R., M.H., M.M., K.K., A.B., J.B., A.S., R.V. & P.S. Visualization – P.H., A.S., & P.S. Supervision – R.V. & P.S. Project Administration – P.S. Acquisition – P.S.

Conflict of Interest: None

Financial Support: This work was funded by the Ministry of Health of the Czech Republic in cooperation with the Czech Health Research Council, grant no. NU22-08-00186 to P.S. and the Grant Agency of Charles University, project no. 307123 to M.O.A; Agentura Pro Zdravotnický Výzkum České Republiky [NU22-08-00186].

Ethics Statement: Experimental protocol of the study was approved by the Institutional Review Boards of the National Institute of Public Health in Prague (approval reference no. IGA NS9803–4 of 2 February 2008), University Hospital Motol (approval reference no. EK-890/15 of 24 June 2015), University Hospital Kralovske Vinohrady (approval reference no. EK-VP/40/0/2017 of 28 June 2017), and University Hospital Pilsen (approval reference no. 16-29013A of 4 June 2015). All patients included in the study read and signed the Patient Informed Consent.

References

1. Cabasag CJ, Fagan PJ, Ferlay J, Vignat J, Laversanne M, Liu L, et al. Ovarian cancer today and tomorrow: a global assessment by world region and human development index using GLOBOCAN 2020. Int J Cancer. 2022;151(9):1535-46.
2. Matulonis UA, Sood AK, Fallowfield L, Howitt BE, Sehouli J, Karlan BY. Ovarian cancer. Nat Rev Dis Primers. 2016;2(1):16061.
3. Matz M, Coleman MP, Carreira H, Salmerón D, Chirlaque MD, Allemani C, et al. Worldwide comparison of ovarian cancer survival: histological group and stage at diagnosis (CONCORD-2). Gynecol Oncol. 2017;144(2):396-404.
4. Kim A, Ueda Y, Naka T, Enomoto T. Therapeutic strategies in epithelial ovarian cancer. J Exp Clin Cancer Res. 2012;31(1):14.
5. American Cancer Society. Ovarian cancer survival rates. Available from: https://www.cancer.org/cancer/types/ovarian-cancer/detection-diagnosis-staging/survival-rates.html
6. Lheureux S, Gourley C, Vergote I, Oza AM. Epithelial ovarian cancer. Lancet. 2019;393(10177):1240-53.
7. Lisio MA, Fu L, Goyeneche A, Gao ZH, Telleria C. High-grade serous ovarian cancer: basic sciences, clinical and therapeutic standpoints. Int J Mol Sci. 2019;20(4):952.
8. Cortez AJ, Tudrej P, Kujawa KA, Lisowska KM. Advances in ovarian cancer therapy. Cancer Chemother Pharmacol. 2018;81(1):17-38.
9. O'Sullivan Coyne G, Chen AP, Meehan R, Doroshow JH. PARP inhibitors in reproductive system cancers: current use and developments. Drugs. 2017;77(2):113-30.
10. Banerjee S, Gonzalez-Martin A, Harter P, Lorusso D, Moore KN, Oaknin A, et al. First-line PARP inhibitors in ovarian cancer: summary of an ESMO Open-Cancer Horizons round-table discussion. ESMO Open. 2020;5(6):e001110.
11. Chartron E, Theillet C, Guiu S, Jacot W. Targeting homologous repair deficiency in breast and ovarian cancers: biological pathways, preclinical and clinical data. Crit Rev Oncol Hematol. 2019;133:58-73.
12. Rojas V, Hirshfield KM, Ganesan S, Rodriguez-Rodriguez L. Molecular characterization of epithelial ovarian cancer: implications for diagnosis and treatment. Int J Mol Sci. 2016;17(12):2113.
13. Goyal G, Fan T, Silberstein PT. Hereditary cancer syndromes: utilizing DNA repair deficiency as therapeutic target. Fam Cancer. 2016;15(3):359-66.
14. Hlaváč V, Holý P, Václavíková R, Rob L, Hruda M, Mrhalová M, et al. Whole-exome sequencing of epithelial ovarian carcinomas differing in resistance to platinum therapy. Life Sci Alliance. 2022;5(12):e202201551.
15. Norquist BM, Brady MF, Harrell MI, Walsh T, Lee MK, Gulsuner S, et al. Mutations in homologous recombination genes and outcomes in ovarian carcinoma patients in GOG 218: an NRG Oncology/Gynecologic Oncology Group study. Clin Cancer Res. 2018;24(4):777-83.
16. Zhang H, Liu T, Zhang Z, Payne SH, Zhang B, McDermott JE, et al. Integrated proteogenomic characterization of human high-grade serous ovarian cancer. Cell. 2016;166(3):755-65.
17. Li C, Bonazzoli E, Bellone S, Choi J, Dong W, Menderes G, et al. Mutational landscape of primary, metastatic, and recurrent ovarian cancer reveals c-MYC gains as potential target for BET inhibitors. Proc Natl Acad Sci U S A. 2019;116(2):619-24.
18. de Witte CJ, Kutzera J, van Hoeck A, Nguyen L, Boere IA, Jalving M, et al. Distinct genomic profiles are associated with treatment response and survival in ovarian cancer. Cancers (Basel). 2022;14(6):1511.
19. Pejovic T, Fitch K, Mills G. Ovarian cancer recurrence: is the definition of platinum resistance modified by PARP inhibitors and other intervening treatments? Cancer Drug Resist. 2022;5:451-8.
20. Friedlander M, Trimble E, Tinker A, Alberts D, Avall-Lundqvist E, Brady M, et al. Clinical trials in recurrent ovarian cancer. Int J Gynecol Cancer. 2011;21(4):771-5.
21. Souček P, Anzenbacher P, Skoumalova I, Dvorak M. Expression of cytochrome P450 genes in CD34+ hematopoietic stem and progenitor cells. Stem Cells. 2005;23(9):1417-22.
22. Elsnerova K, Mohelnikova-Duchonova B, Cerovska E, Ehrlichova M, Gut I, Rob L, et al. Gene expression of membrane transporters: importance for prognosis and progression of ovarian carcinoma. Oncol Rep. 2016;35(4):2159-70.
23. Bustin SA, Benes V, Garson JA, Hellemans J, Huggett J, Kubista M, et al. The MIQE guidelines: minimum information for publication of quantitative real-time PCR experiments. Clin Chem. 2009;55(4):611-22.

24. Livak KJ, Schmittgen TD. Analysis of relative gene expression data using real-time quantitative PCR and the 2−ΔΔCT method. Methods. 2001;25(4):402-8.
25. Untergasser A, Cutcutache I, Koressaar T, Ye J, Faircloth BC, Remm M, et al. Primer3—new capabilities and interfaces. Nucleic Acids Res. 2012;40(15):e115.
26. André F, Arnedos M, Baras AS, Baselga J, Bedard PL, Berger MF, et al. AACR Project GENIE: powering precision medicine through an international consortium. Cancer Discov. 2017;7(8):818-31.
27. Mohammad AI, Obeed Allah M, Ali E, Krus I, Šůsová S, Tesařová T, et al. Functional validation of somatic variability in TP53 and KRAS for prediction of platinum sensitivity and prognosis in epithelial ovarian carcinoma patients. Int J Cancer. 2024;155(1):104-16.
28. Nasioudis D, Fernandez ML, Wong N, Powell DJ Jr, Mills GB, Westin S, et al. The spectrum of MAPK-ERK pathway genomic alterations in gynecologic malignancies: opportunities for novel therapeutic approaches. Gynecol Oncol. 2023;177:86-94.
29. Therachiyil L, Anand A, Azmi A, Bhat A, Korashy HM, Uddin S. Role of RAS signaling in ovarian cancer. F1000Res. 2022;11:1253.
30. Peres LC, Cushing-Haugen KL, Köbel M, Harris HR, Berchuck A, Rossing MA, et al. Invasive epithelial ovarian cancer survival by histotype and disease stage. J Natl Cancer Inst. 2019;111(1):60-8.
31. Stewart J, Cunningham N, Banerjee S. New therapies for clear cell ovarian carcinoma. Int J Gynecol Cancer. 2023;33(3):385-93.
32. Tang D, Kang R. Glimmers of hope for targeting oncogenic KRAS-G12D. Cancer Gene Ther. 2023;30:391-3.
33. Kim D, Herdeis L, Rudolph D, Zhao Y, Böttcher J, Vides A, et al. Pan-KRAS inhibitor disables oncogenic signalling and tumour growth. Nature. 2023;619(7968):160-6.
34. Nakajima EC, Drezner N, Li X, Mishra-Kalyani PS, Liu Y, Zhao H, et al. FDA approval summary: sotorasib for KRAS G12C-mutated metastatic NSCLC. Clin Cancer Res. 2022;28(8):1482-6.
35. Dhillon S. Adagrasib: first approval. Drugs. 2023;83(3):275-85.
36. Brachova P, Mueting SR, Carlson MJ, Goodheart MJ, Button AM, Mott SL, et al. TP53 oncomorphic mutations predict resistance to platinum- and taxane-based standard chemotherapy in patients diagnosed with advanced serous ovarian carcinoma. Int J Oncol. 2015;46(2):607-18.
37. Peuget S, Zhou X, Selivanova G. Translating p53-based therapies for cancer into the clinic. Nat Rev Cancer. 2024;24(3):192-215.
38. Dong ZY, Zhong WZ, Zhang XC, Su J, Xie Z, Liu SY, et al. Potential predictive value of TP53 and KRAS mutation status for response to PD-1 blockade immunotherapy in lung adenocarcinoma. Clin Cancer Res. 2017;23(12):3012-24.
39. Gu M, Xu T, Chang P. KRAS/LKB1 and KRAS/TP53 co-mutations create divergent immune signatures in lung adenocarcinomas. Ther Adv Med Oncol. 2021;13:17588359211006950.
40. Datta J, Bianchi A, De Castro Silva I, Deshpande NU, Cao LL, Mehra S, et al. Distinct mechanisms of innate and adaptive immune regulation underlie poor oncologic outcomes associated with KRAS-TP53 co-alteration in pancreatic cancer. Oncogene. 2022;41(28):3640-54.
41. Rechsteiner M, Zimmermann AK, Wild PJ, Caduff R, von Teichman A, Fink D, et al. TP53 mutations are common in all subtypes of epithelial ovarian cancer and occur concomitantly with KRAS mutations in the mucinous type. Exp Mol Pathol. 2013;95(2):235-41.
42. Soberanis Pina P, Lheureux S. Overcoming PARP inhibitor resistance in ovarian cancer. Int J Gynecol Cancer. 2023;33(3):364-76.
43. Coelho R, Tozzi A, Disler M, Lombardo F, Fedier A, López MN, et al. Overlapping gene dependencies for PARP inhibitors and carboplatin response identified by functional CRISPR-Cas9 screening in ovarian cancer. Cell Death Dis. 2022;13(10):909.
44. McMullen M, Karakasis K, Madariaga A, Oza AM. Overcoming platinum and PARP-inhibitor resistance in ovarian cancer. Cancers (Basel). 2020;12(6):1607.